Preparation of Biomorphic TiO_2 Ceramics from Rattan Templates

Liangcun Qian,[a,b,c] Rui Li,[a,b] Liang Zhou,[a] Yamei Liu,[a] Min Yu,[a] Fuquan Xiong,[a] Shengquan Liu,[a,]* and Xiaotao Hao [c,]*

In this work, biomorphic ceramics were produced from various rattan templates, and sol infiltration was used with vacuum/positive pressure technology. Finally, the samples were sintered to form TiO_2 ceramics with a rattan microstructure. Through X-ray diffraction (XRD), thermogravimetric (TG) data, dimensional variation analysis, and scanning electron microscopy (SEM) images of biomorphic ceramics, the results of this experiment showed that the times of sol-gel infiltration were decreased due to use of the vacuum/positive pressure technology. In order to further supply the TiO_2 content and fill the pyrolysis gaps in the charcoal/TiO_2 composites sintered at 800 °C, it was necessary to repeat the sol-gel process. In the transverse section, ceramics for the rattan templates without the rattan edge, more perfect biomorphic features were achieved. Conversely, deformations occurred along the transverse section of the ceramics for the templates made with the rattan edge. Meanwhile, the fracture phenomenon took place along the ceramic axial section. The main reason for deformation and fracture was that the anisotropic structure of the template was stressed during the sintering process. Furthermore, the micrometer-sized pores were found in the ceramics along the axial section because of the removal of the charcoal templates.

Keywords: Biomorphic ceramic; Charcoal template; Fracture behavior; Rattan; Anisotropic structure

Contact information: a: College of Forestry and Gardening, Anhui Agricultural University, Hefei 230036, P. R. China; b: School of Science, Anhui Agricultural University, Hefei, 230036, P.R. China; c: School of Physics, Shandong University, Jinan, 250100, P.R. China;
** Corresponding authors: liusq@ahau.edu.cn; haoxt@sdu.edu.cn*

INTRODUCTION

Biomorphic porous ceramics are suitable for use as sensors (Lohr *et al.* 2013; Abdullah *et al.* 2014), catalytic packing for novel reactors (Luo *et al.* 2007), and absorption/separation units (Zampieri *et al.* 2005). Bio-templates of rattan stem with the microstructure of natural growing plants are of particular interest to material scientists for producing biomorphic materials. The inherently open pores from the natural anatomy of the structures are accessible for gaseous or aqueous infiltration, and the structure is additionally suitable for bio-templates of biomorphic porous ceramics (Ohji and Fukushima 2012). However, it is evident that porous ceramics from bio-charcoal templates are more prone to collapse and cracking during the sintering process. And few studies have reported the fracture behavior of charcoal templates or the fracture formation mechanism during sintering of biomorphic ceramics (Mizutani *et al.* 2005).

The compound TiO_2 is one of the most promising semiconductor photocatalysts (Espinosa *et al.* 2005) because it has the advantages of being non-toxic, antibacterial, and exceptionally hydrophilic (Kallio *et al.* 2006; Bahloul *et al.* 2012; Qin and Zhang 2012; Sun *et al.* 2013; Liu *et al.* 2014). During the calcination of TiO_2 ceramics below 1200 °C in an air or nitrogen atmosphere, the contact area between the TiO_2 crystal grains is limited, resulting in a lower bonding strength. Therefore, the formation of the TiO_2 crystal phase is controllable (Cao *et al.* 2004).

The anisotropic properties can be compared as the differences of density, anatomic structure, and shrinkage rate (SR) depending on the kinds of processes along different directions or in different positions. The anisotropic properties of native rattan are remarkably different between the radial and axial dimensions. (Jiang 2010; Balakrishna *et al.* 2013). On the transverse section from the center to the edge, the diameter of vessels decreases stepwise. The geometrical density of the rattan edge is larger than that of the center in a rattan stem. The average geometrical densities of the center and the rattan edge are about 0.2 g/cm^3 and 0.7 g/cm^3, respectively. Therefore, in this paper, fracture behavior from biomorphic TiO_2 ceramics and charcoal/TiO_2 composites (C/TiO_2) is reported using the microstructure analysis of rattan templates with different dimensions. Furthermore, infiltration behavior of the different templates and the TiO_2 phase formation are analyzed to discover the crack mechanism of biomorphic TiO_2 ceramics.

Cao *et al.* (2004) sintered biomorphic TiO_2 ceramics with pine tamplates after sol-gel infiltration by vacuum technology, but butyl titanate ($Ti(OC_4H_9)_4$) for sol-gel infiltration was repeated up to more than three times. In order to decrease the times of sol-gel infiltration, vacuum/positive pressure technology was warranted. Moreover different rattan samples were used as templates for producing biomorphic ceramics. Finally, X-ray diffraction (XRD), thermogravimetric (TG) data, scanning electron microscopy (SEM) images, and dimensional variations were investigated to evaluate the biomorphic TiO_2 ceramics.

EXPERIMENTAL

Materials

$Ti(OC_4H_9)_4$ was supplied by Kemiou Chemical Reagent Co. Ltd., Tianjin, China. Acetic acid (CH_3COOH), benzene (C_6H_6), and anhydrous ethanol (CH_3CH_2OH) were supplied by Sinopharm Chemical Reagent Co. Ltd., Shanghai, China. All reagents were of analytical grade and did not require further purification. The purity of nitrogen (N_2) was 99.999%.

Specimens of rattan (*Calamus simplicifolius*) were obtained from Yingyang Forest Farm in Pingxiang County, Guangxi Zhuang autonomous region, China. Rattan specimens were sawn into cylinder (including the rattan edge along the axial direction) transverse sections with a thickness of 8.67 ± 0.01 mm and an average diameter of 19.88 ± 0.02 mm (S1). In addition, rattan specimens were sawn into cylinder (excluding the rattan edge) transverse sections with a thickness of 8.67 ± 0.01 mm and an average diameter of 15.86 ± 0.02 mm (S2).

Methods

Pretreatment process

All rattan samples were vacuum-dried at 60 °C for 24 h and pretreated in a Soxhlet apparatus with benzene-alcohol mixture (volume ratio of C_6H_6: 95% CH_3CH_2OH = 1:2) at 90 °C for 6 h under reflux to remove any extractives (fats and fatty acids) from the samples. Then, all of the samples were oven-dried at 90 °C for 24 h.

Sol-gel infiltration process

$Ti(OC_4H_9)_4$, CH_3COOH, and CH_3CH_2OH, with a volume ratio of 68:12:50, were stirred for 2 h at room temperature to obtain the TiO_2 sol. The extracted samples were immersed in the TiO_2 sol for six days and subsequently subjected to infiltration in an adjustable air pressure dipping can at a pressure of 1.00 kPa for 30 min and then at a positive air pressure of 2.00 MPa for 30 min. Finally, all of the samples were taken out from the TiO_2 sol. The TiO_2 sol absorbed water from the air for 12 h, resulting in the formation of $Ti(OC_4H_9)_4$ gel. Gel and the samples were heated to 130 °C by increasing the temperature stepwise; in addition 130 °C was maintained for 2 h. The infiltration-drying process was repeated two times to increase the gel content in the samples.

Annealing process

A furnace containing a vacuum tube (GLS-1400X, Kexing Materials Co. Ltd., China) was used for sintering the samples. The temperature program was set as follows: 20 to 400 °C at a heating rate of 1 °C min^{-1}, 400 °C to the maximum temperature (800 °C in N_2 or 1200 °C in air) at a heating rate of 2 °C min^{-1}, maintaining the maximum temperature for 1 h, and decreasing from the maximum temperature to room temperature at a cooling rate of -2 °C min^{-1}. After the infiltration process, the samples were pyrolyzed to produce porous C/TiO_2 at 800 °C for 1 h in a N_2 atmosphere (Sun *et al.* 2004; Mizutani *et al.* 2005; Istomina *et al.* 2013). Further infiltration steps were performed to increase the TiO_2 content in the C/TiO_2 porous templates. Subsequently, the sol-gel process was repeated in the samples. In the end, the specimens were annealed to remove the charcoal templates, and biomorphic TiO_2 ceramics were formed in an air atmosphere at 1200 °C for 1 h. The processing route for producing biomorphic TiO_2 ceramics is summarized in Fig. 1.

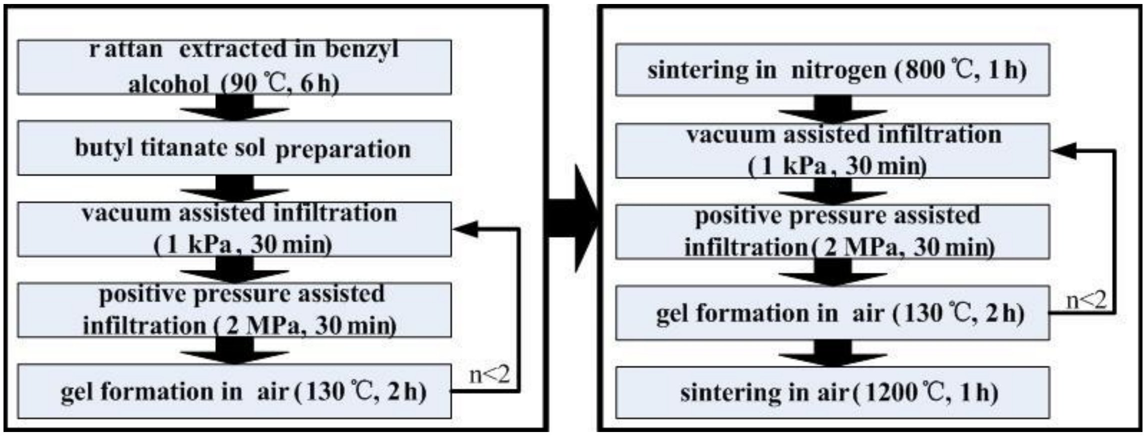

Fig. 1. Flow chart for the manufacturing of biomorphic TiO_2 ceramics from rattan templates

Characterization

The phase formation during processing was identified using an X-ray diffractometer (XD-3, Puxi, China) operating under Cu Kα radiation (λ = 15.40563 nm), with a scan rate of 1°/min, accelerating voltage of 36 kV, applied current of 20 mA, and diffraction angle (2θ) ranging from 10° to 70°.

The microstructures of the infiltrated rattan samples, biomorphic charcoals, C/TiO_2, and TiO_2 ceramics were observed using scanning electron microscopy (SEM, HITACHI, Japan).

The mass (M) of samples was measured using a balance with the precision of 0.001 g, and the volume (V) of samples was measured using vernier calipers with a precision of 0.01 mm. Densities (ρ g/cm^3) were calculated using Eq. 1:

$$\rho = \frac{M}{V} \tag{1}$$

The dimensions of the samples always shrunk during the annealing process. Therefore, the dimensions of native samples (L_0) and annealed samples (L) were measured, and the shrinkage rates (SR %) were calculated using Eq. 2:

$$SR = \frac{L_0 - L}{L_0} \times 100\% \tag{2}$$

A thermogravimetric analyzer (TGA-209, NETZSCH, Germany) was used to analyze the mass loss (ΔM) of C/TiO_2, operating with purge air at an air flow rate of 20 mL/min. Ten milligrams of C/TiO_2 powder was loaded into the alumina crucible of the TGA-209 and was heated at the rate of 10 °C/min from 40 to 700 °C. The slopes of thermogravimetric (TG) profiles were expressed as the speed of mass loss (MS). Therefore, the average speed of MS (slope %/°C) was calculated using Eq. 3, where Δt is the variation of temperature (Δt °C) during mass loss (ΔM %):

$$slope = \frac{\Delta M\%}{\Delta t} \tag{3}$$

RESULTS AND DISCUSSION

Sol-gel Process

The rattan templates were baked at 130 °C for 2 h to remove the ethanol and acetic acid from the samples. The above mentioned sol-gel process was repeated four times on the rattan templates and C/TiO_2. Table 1 shows the physical properties of native, C/TiO_2 composites, and TiO_2 ceramics from rattan. An increase in sample geometric density was observed for the native rattan impregnated with TiO_2 gel from time 1 to 4. Meanwhile, no further increment was observed for the samples from the 3rd impregnation.

In the SEM images, Fig. 2(a) shows the amorphous TiO_2 gel-filled rattan vessels and cell cavities after the first sol-gel process of the transverse section. None of the gel completely sealed the holes in the vessels and cell cavities. But gel filled the spaces of the vessels and cell cavities after the second sol-gel process of the transverse section, as shown in Fig. 2(b).

Table 1. Physical Properties of the Native Rattans, C/TiO_2 Composites, and TiO_2 Ceramics (S1)

Physical properties	Native rattans	C/TiO_2 composites	TiO_2 ceramics
Average diameter (mm)	19.88 ± 0.02	15.54 ± 0.02	14.03 ± 0.02
Average axial thickness (mm)	8.67 ± 0.01	7.66 ± 0.01	7.18 ± 0.01
Un-infiltrated materials density (g/cm^3)	0.503 ± 0.003	0.668 ± 0.003	0.805 ± 0.004
The 1st time infiltrated materials density (g/cm^3)	0.773 ± 0.003	0.807 ± 0.003	--
The 2nd time infiltrated materials density (g/cm^3)	0.816 ± 0.003	0.860 ± 0.004	--
The 3rd time infiltrated materials density (g/cm^3)	0.819 ± 0.004	0.863 ± 0.004	--
The 4th time infiltrated materials density (g/cm^3)	0.820 ± 0.004	0.860 ± 0.004	--

Because heated gelatin always releases gases from acetic acid, ethanol, and butyl alcohol (Sun *et al.* 2004), the rooms were discharged between the mixture of $Ti(OC_4H_9)_4$ gelatin and templates. It was concluded that the impregnated gel nearly reached the saturation state in the vessels and cell cavities of the samples, when the sol-gel process was repeated (by the second impregnation). Therefore, the sol-gel process needed to be repeated twice in the present experiment through vacuum/positive pressure technology.

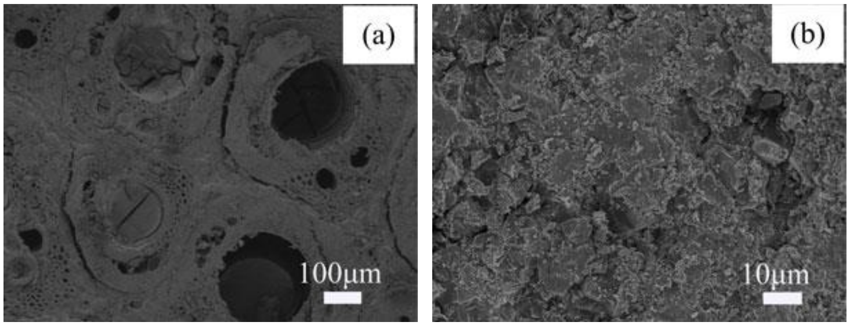

Fig. 2. SEM of the rattan transverse section after sol-gel processing: (a) First sol-gel process, rattan transverse section×100, and (b) the second sol-gel process, rattan transverse section×1.00k

TiO_2-phase Formation

The curve for the TiO_2-phase formation from 350 to 900 °C in air was detected by Cao *et al.* (2004), and rutile TiO_2 started at about 500 °C. Sun *et al.* (2004) concluded that the decomposition from tetrabutyl titanate to anatase TiO_2 started at about 250 °C and rutile TiO_2 mostly occurred between 400 and 600 °C in air. The TiO_2-phase formation of specimens in N_2 between 400 and 1200 °C was monitored by XRD analysis (Fig. 3). The diffraction peaks at 25.2°, 37.8°, 48.1°, and 55.2° could be assigned to the diffractions of the (101), (004), (200), and (211) planes of anatase TiO_2 (JCPDS number 21-1272) (Chen and Mao 2007). The diffraction peaks at 27.5°, 36.0°, 41.5°, and 54.0° could be assigned to the diffractions of the (110), (101), (200), and (211) planes of rutile TiO_2 (JCPDS number 21-1276) (Yang *et al.* 2009). The anatase structure was observed at 400 °C. The phase transformation shifted from anatase to rutile between 700 and 800 °C; consequently, the TiO_2-phase was completely rutile in structure at 900 °C. Pyrolysis of the rattan chips (cellulose, hemicelluloses, and lignin) and the formation of TiO_2 phase structures happened simultaneously from 400 to 800 °C in N_2. As the temperature increased, the diffraction peaks of TiO_2 became steeper; pyrolysis of the rattan chips aggravated. Considering critical points of rutile structure and pyrolyzing extent of the samples, it was determined that the sol-gel process of the C/TiO_2 composites sintered at 800 °C was repeated to compensate for templates of mass loss (MS) because of volatilized carbon.

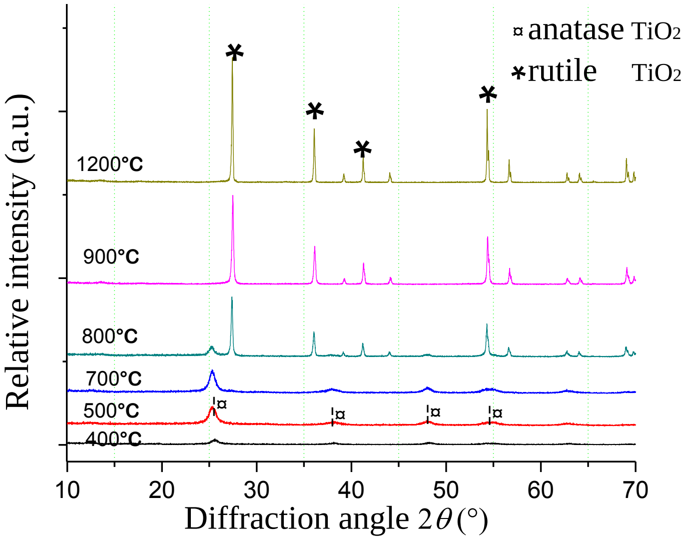

Fig. 3. The XRD patterns of the charcoal/TiO_2 composites annealed at various temperatures in N_2

Thermogravimetric Analysis

In order to investigate the thermo-stability of C/TiO_2 composites, the C/TiO_2 composites were sintered at 400 °C (400C/TiO_2) and 800 °C (800C/TiO_2) in N_2. Oxygenolysis curves below 700 °C in TGA-209 are shown in Fig. 4. Comparing TG curves of 400C/TiO_2 and 800C/TiO_2, the corresponding remnants (TiO_2) were estimated to be approximately 61.80% and 69.06%, respectively, and the corresponding temperatures for removal of the charcoal templates were approximately 580 and 650 °C, respectively. From the approximately level curves of 400C/TiO_2 and 800C/TiO_2, it can be concluded that the two composites were stable in air below 350 °C. The approximately equal MS rate of 400C/TiO_2 showed that C/TiO_2 oxygenolysis and TiO_2-phase formation happened smoothly below 580 °C and terminated at approximately 580 °C. From the slopes of the TG profiles, the four average slopes calculated using Eq. 3 were slope 1 (0.1550%/°C), slope 2 (0.0625%/°C), slope 3 (0.2491%/°C), and slope 4 (0.1107%/°C), respectively. The MS rate of the 400C/TiO_2 between 350 and 580 °C was obviously faster than that of the 800C/TiO_2 between 350 and 650 °C. Although the MS rate of the 800C/TiO_2 was slower than that of the 400C/TiO_2 between 350 and 580 °C, the MS rate of the 800C/TiO_2 between 580 and 650 °C was faster than that of the 800C/TiO_2 between 350 and 580 °C. In addition, during oxygenolysis, the 800C/TiO_2 lagged behind that of the 400C/TiO_2. It can be speculated that the TiO_2 on the surface of the 800C/TiO_2 composites hindered the oxygenolysis below 580 °C because TiO_2 was tightly packed around charcoal. On the other hand, the TiO_2 on the surface of the 800C/TiO_2 composites enhance the capacity for oxygenolysis beyond 580 °C because of the oxygenolysis gaps between charcoal and TiO_2 in the 800C/TiO_2 composites (Sun *et al.* 2010). The 800C/TiO_2 composites is more stable than the 400C/TiO_2 composites in air, so it was necessary to repeat the sol-gel process in order to further supply the TiO_2 content and to fill the possible oxygenolysis gaps in the composites sintered at 800 °C.

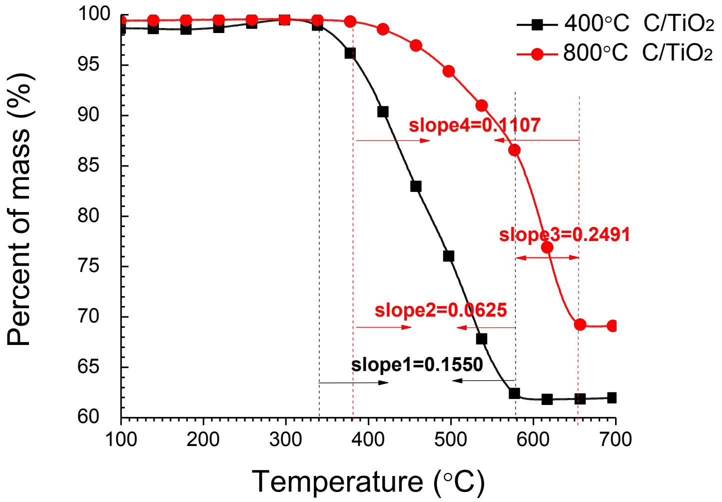

Fig. 4. The mass loss (MS) rate of C/TiO_2 composites at 400 and 800 °C by TG analysis in air

Dimension Variation of Annealed Samples

In porous materials, the pore-size distribution is very important. The native rattan stem has a complex pipe and pore system, and Mizutani and Eichenseer *et al.* investigated into the pore-size distribution from rattan palm to bioinspired monoliths by porosity measures (Mizutani *et al.* 2005; Eichenseer *et al.* 2010). Therefore in order to discover the SR anisotropy in the rattan templates, the different kinds of pores were displayed and measured further along the axial and transverse section. The charcoals pyrolyzed from rattan at 800 °C in N_2 without impregnation exhibited multi-scale anatomy structures, as shown in Fig. 5. All of the pores retained the anatomic structure of rattan effectively. In Fig. 5(a) the diameter of vessels, sieve tubes, and fiber cells on the rattan charcoal transverse section were approximately 200, 50, and 2 μm, respectively. Figure 5(b) displays successive vessel, sieve tube, fiber, and parenchyma orientation from left to right along the axial section. Many starch particles without any pores on the sieve tube wall and a few apertures with a pore size of approximately 1 μm on the fiber cell walls were found. In addition, parenchyma tissue exhibited the largest pores (~ 10 μm) and the smallest apertures (~ 2 μm). The pit sizes of the rattan charcoals along the axial section in the vessel wall were approximately 1 to 5 μm (Fig. 5c). The charcoal templates from the native rattan composites were notably anisotropic along the radial and axial sections; however, no fracture phenomena were found along these sections under 4.00k magnification after calcination. The anatomical structure of the 800C/TiO_2 is shown in Fig. 6. Most diameters of big vessels were reduced to approximate 3/4 of the original dimensions (< 150 μm) in the transverse sections. Table 1 shows the dimensional variation from the native rattan, 800C/TiO_2, and ceramics, respectively. In Eq. 2 the SR of impregnated rattans sintered to 800C/TiO_2, and ceramic along the radial direction was 21.8% and 29.5%, respectively. The axial SR was 11.7% and 17.2%, respectively. However, the radial SR and axial SR were 9.7% and 9.9%, respectively, for the

800C/TiO_2 to ceramic. Hence, the radial SR for impregnated rattans to 800C/TiO_2 were almost twice that of the axial, while for the 800C/TiO_2 to ceramic, the radial SR were approximately equal to the axial SR. As a result, the SR of rattan templates was definitively anisotropic along the radial and axial directions after sintering to forming 800C/TiO_2, while the SR anisotropy nearly disappeared from the 800C/TiO_2 to ceramic.

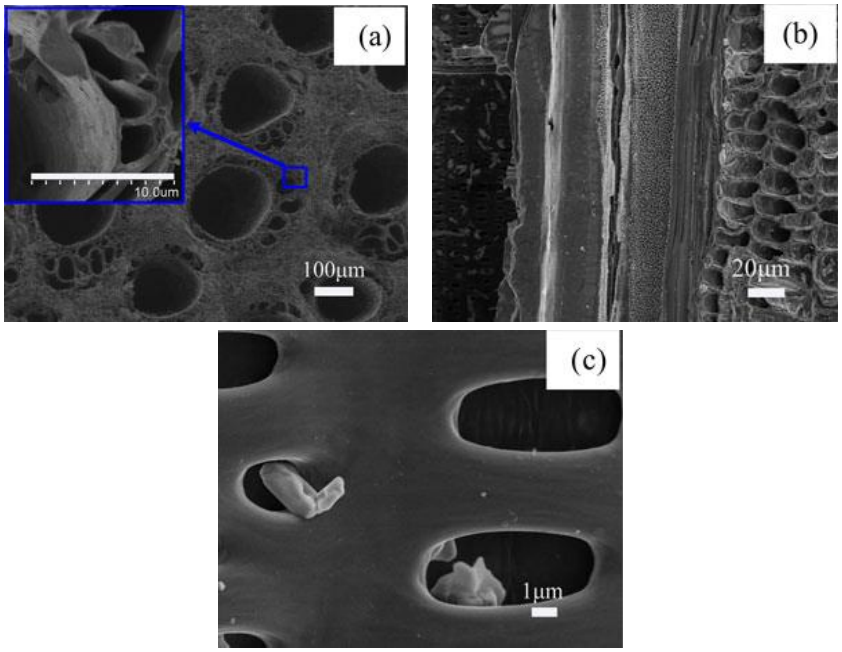

Fig. 5. The SEM images of rattan charcoal after sintering at 800 °C in N_2: (a) transverse section of rattan charcoal×100, top-left transverse section of rattan charcoal×4.00k; (b) axial section of rattan charcoal ×500; (c) pits in the vessel, vessel×6.00k

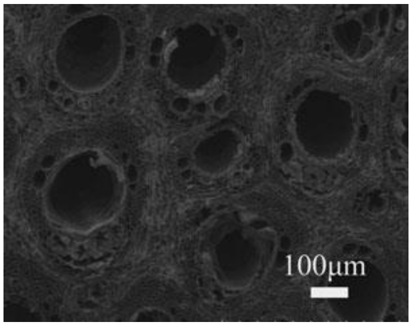

Fig. 6. The SEM image of the C-TiO_2 composite material's transverse section×100 derived from rattan after sintering at 800 °C in N_2

Because of the anisotropic structure of the bio-templates, further removal of the S1 and S2 bio-templates from C/TiO_2 may have resulted in the fracture and deformation of the ceramic (Jiang 2010; Eichenseer *et al.* 2010). SEM images of the biomorphic ceramic are displayed in Fig. 7 (S1) and Fig. 8 (S2). Figure 7(a) shows deformation in the microstructure of the transverse section of the ceramic from S1, and Fig. 7(b) exhibited cracks in the microstructure in the axial section of the ceramic from S1. However, biomorphic ceramic from S2 more perfectly performed the biomorphic feature of rattan templates both in transverse section and in axial section as Fig. 8. Figure 8(a) shows the

SEM image from the transverse section of biomorphic ceramic from S2. Figures 8(b) and (c) are SEM images from the axial section of the biomorphic ceramic S2. Both the ceramic sections perfectly matched the bio-templates from the native rattan. This was because removal of the rattan edge from both of the ceramic sections successfully prevented the thermo-stress of the anisotropic structure over the course of the sintering process from native rattan to biomorphic ceramic. Therefore, this suggests that the rattan templates should cut off the rattan edge of the rattan stem to obtain biomorphic TiO_2 ceramics from rattan. In Fig. 8(c), another kind of micrometer scale pores was found in the ceramics' axial sections, and these pores did not originate from the textures of the charcoal templates. These pores may have developed because of the continuous removal of the charcoal templates during the sintering process.

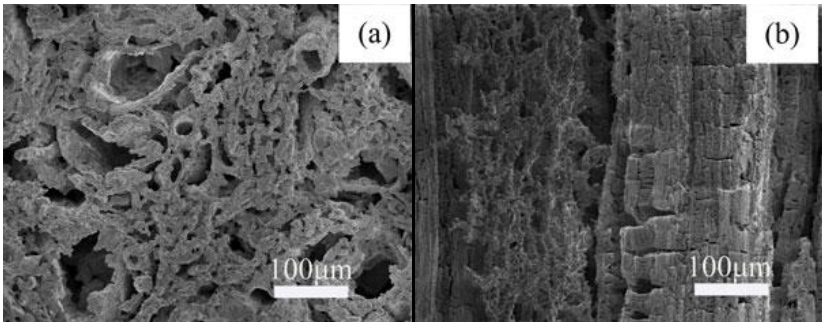

Fig. 7. The SEM micrographs of the porous TiO_2 ceramics derived from S1 rattan after sintering at 1200 °C in air: (a) transverse section×200, and (b) axial section×200

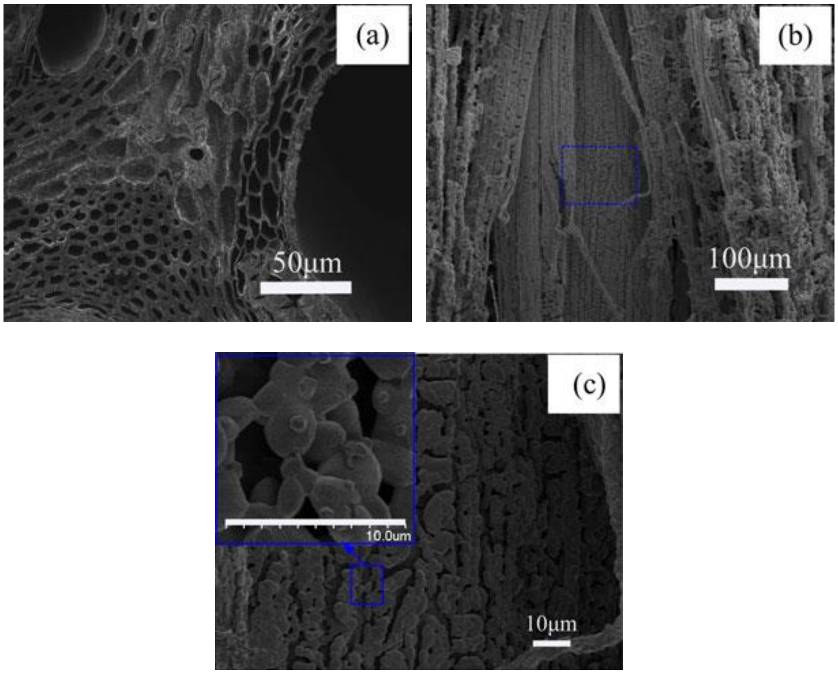

Fig. 8. The SEM micrographs of the biomorphic TiO_2 ceramics derived from S2 rattan without the rattan edge after sintering at 1200 °C in air: (a) transverse section ×500, (b) axial section ×200, and (c) axial section ×1.00k & middle of transverse section ×5.00k

CONCLUSIONS

1. Because of the continuous volatilization of small molecules from the bio-templates, it was necessary to supply TiO_2 gel to the bio-charcoal templates sintered at 800 °C, and impregnation of TiO_2 gel was greater than 60% of the templates mass.
2. The TiO_2 ceramics performed biomorphic pores of the rattan templates along the transverse section. Moreover many micrometer-sized pores in the ceramics originated from the axial section because of removal of the charcoal templates.
3. Because the anatomic structure of the bio-templates is definitively anisotropic in nature, removal of the charcoal templates makes the biomorphic TiO_2 ceramics and C/TiO_2 composites more prone to fracture and deformation. Symmetric templates, excluding the rattan edge, are required to overcome shrinkage stress for sintering.

ACKNOWLEDGEMENT

This work was financially supported by the National Key Technology R&D Program in the 12th Five-year Plan of China (No. 2014BAK09B03), the Cultured Subject Program of Anhui Agricultural University in China (No. 2014XKPY-36), and the Visiting Scholar Project to Youth Teachers from Institutions of Higher Education in China.

REFERENCES CITED

Abdullah, M., and Rusop, M. (2014). "RF sputtered tri-functional antireflective TiO_2 (arc-TiO_2) compact layer for performance enhancement in dye-sensitised solar cell," *Ceramics International* 40(1), 967-974. DOI: 10.1016/j.ceramint.2013.06.093

Bahloul, W., Mélis, F., Bounor-Legaré, V., and Cassagnau, P. (2012). "Structural characterisation and antibacterial activity of PP/TiO_2 nanocomposites prepared by an *in situ* sol–gel method," *Materials Chemistry and Physics* 134(1), 399-406. DOI: 10.1016/j.matchemphys.2012.03.008

Balakrishna, N. S., Ismail, H., and Othman, N. (2013). "Processing, mechanical, and thermal properties of polypropylene/rattan powder/talc hybrid composites," *BioResources* 8(4), 6409-6423. DOI: 10.15376/biores.8.4.6409-6423

Cao, J., Rusina, O., and Sieber, H. (2004). "Processing of porous TiO_2-ceramics from biological preforms," *Ceramics International* 30(7), 1971-1974. DOI: 10.1016/j.ceramint.2003.12.180

Chen, X., and Mao, S. S. (2007). "Titanium dioxide nanomaterials: Synthesis, properties, modifications, and applications," *Chemical Reviews* 107(7), 2891-2959. DOI: 10.1021/cr0500535

Eichenseer, C., Will, J., Rampf, M., Wend, S., and Greil, P. (2010). "Biomorphous porous hydroxyapatite-ceramics from rattan (*Calamus rotang*)," *Journal of Materials Science: Materials in Medicine* 21(1), 131-137. DOI: 10.1007/s10856-009-3857-3

Espinosa, R., Zumeta, I., Santana, J. L., Martínez-Luzardo, F., González, B., Docteur, S., and Vigil, E. (2005). "Nanocrystalline TiO_2 photosensitized with natural polymers with enhanced efficiency from 400 to 600 nm," *Solar Energy Materials and Solar Cells* 85(3), 359-369. DOI: 10.1016/j.solmat.2004.05.006

Istomina, E., Istomin, P., and Nadutkin, A. (2013). "Preparation of biomorphic SiC," *Inorganic Materials* 49(10), 984-987. DOI: 10.1134/S0020168513090070

Jiang, Z. H. (2010). "Analysis of the microfibrilla angles & crystallinity index of daemonorops margaritae with X-ray diffractometry and the effects of γ-ray irradiation," *Spectroscopy and Spectral Analysis* 30(5), 1404-1407. DOI: 10.3964/j.issn.1000-0593(2010)08-2285-04

Kallio, T., Alajoki, S., Pore, V., Ritala, M., Laine, J., Leskelä, M., and Stenius, P. (2006). "Antifouling properties of TiO_2: Photocatalytic decomposition and adhesion of fatty and rosin acids, sterols and lipophilic wood extractives," *Colloids and Surfaces A: Physicochemical and Engineering Aspects* 291(1), 162-176. DOI: 10.1016/j.colsurfa.2006.06.044

Liu, C., Li, Y., Wei, L., Wu, C., Chen, Y., Mei, L., and Jiao, J. (2014). "CdS quantum dot-sensitized solar cells based on nano-branched TiO_2 arrays," *Nanoscale Research Letters* 9(1), 1-8. DOI: 10.1186/1556-276X-9-107

Lohr, J., Treusch, O. G., Standfest, G., Petutschnigg, A., Wieland, S., and Wegener, G. (2013). "Production process of wood-based materials for SiC ceramics," *European Journal of Wood and Wood Products* 71(4), 417-428. DOI: 10.1007/s00107-013-0692-5

Luo, M., Gao, J., Zhang, X., Hou, G., Yang, J., Ouyang, D., Wang, H., and Jin, Z. (2007). "Biomorphic TiN/C ceramics prepared by reduction–nitridation of charcoal/titania composite," *Journal of Materials Science* 42(11), 3761-3766. DOI: 10.1007/s10853-006-0425-9

Mizutani, M., Takase, H., Adachi, N., Ota, T., Daimon, K., and Hikichi, Y. (2005). "Porous ceramics prepared by mimicking silicified wood," *Science and Technology of Advanced Materials* 6(1), 76-83. DOI: 10.1016/j.stam.2004.08.004

Ohji, T., and Fukushima, M. (2012). "Macro-porous ceramics: Processing and properties," *International Materials Reviews* 57(2), 115-131. DOI: 10.1179/1743280411Y.0000000006

Qin, C., and Zhang, W. (2012). "Antibacterial property of titanium alkoxide/poplar wood composite prepared by sol-gel process," *Materials Letters* 89(2012), 101-103. DOI: 10.1016/j.matlet.2012.08.089

Sun, B., Fan, T., and Zhang, D. (2004). "Production of morph-genetic TiC/C ceramic," *Materials Letters* 58(5), 798-801. DOI: 10.1016/j.matlet.2003.07.015

Sun, Q., Lu, Y., Tu, J., Yang, D., Cao, J., and Li, J. (2013). "Bulky macroporous TiO_2 photocatalyst with cellular structure via facile wood-template method," *International Journal of Photoenergy* 2013, 649540. DOI: 10.1155/2013/649540

Sun, Q., Yu, H., Liu, Y., Li, J., Cui, Y., and Lu, Y. (2010). "Prolonging the combustion duration of wood by TiO_2 coating synthesized using cosolvent-controlled hydrothermal method," *Journal of Materials Science* 45(24), 6661-6667. DOI: 10.1007/s10853-010-4758-z

Yang, D., Liu, H., Zheng, Z., Yuan, Y., Zhao, J. C., Waclawik, E. R., Ke, X., and Zhu, H. (2009). "An efficient photocatalyst structure: TiO_2 (B) nanofibers with a shell of anatase nanocrystals," *Journal of the American Chemical Society* 131(49), 17885-17893. DOI: 10.1021/ja906774k

Zampieri, A., Sieber, H., Selvam, T., Mabande, G. T., Schwieger, W., Scheffler, F., Scheffler, M., and Greil, P. (2005). "Biomorphic cellular SiSiC/zeolite ceramic composites: From rattan palm to bioinspired structured monoliths for catalysis and sorption," *Advanced Materials* 17(3), 344-349. DOI: 10.1002/adma.200400672

Article submitted: March 6, 2015; Peer review completed: May 15, 2015; Revised version received and accepted: May 25, 2015; Published: May 28, 2015.
DOI: 10.15376/biores.10.3.4391-4402